arXiv:1504.04608v1 [cond-mat.stat-mech] 17 Apr 2015

Influence of disordered porous media in the anomalous properties of a simple water model

A. P. Furlan [a],[1] Carlos E. Fiore [b],[2] and M. C. B. Barbosa [c]3

[1] *Instituto de Física, Univeridade Federal do Rio Grande do Sul, Caixa Postal 15051, 91501-570, Porto Alegre, RS, Brazil.*

[2] *Instituto de Física, Universidade de São Paulo, Caixa Postal 19044, 81531 São Paulo, SP, Brazil.*

[3] *Instituto de Física, Univeridade Federal do Rio Grande do Sul, Caixa Postal 15051, 91501-570, Porto Alegre, RS, Brazil.*

(Dated: April 20, 2015)

Abstract

The thermodynamic, dynamic and structural behavior of a water-like system confined in a matrix is analyzed for increasing confining geometries. The liquid is modeled by a two dimensional associating lattice gas model that exhibits density and diffusion anomalies, in similarity to the anomalies present in liquid water. The matrix is a triangular lattice in which fixed obstacles impose restrictions to the occupation of the particles. We show that obstacules shortens all lines, including the phase coexistence, the critical and the anomalous lines. The inclusion of a very dense matrix not only suppress the anomalies but also the liquid-liquid critical point.

PACS numbers: 61.20.Gy,65.20.+w

[a] email - furlan@if.ufrgs.br

[b] email - fiore@if.usp.br

[c] marcia.barbosa@ufrgs.br

I. INTRODUCTION

The phase behavior of systems as particles interacting via the so-called core-softened (CS) potentials has received a lot of attention recently. They show a repulsive core with a softening region when particles are very close and an attractive region when particles are more distant. These CS can be modeled as continuous potentials or lattice gas models. For the lattice structure the two competing scales arise from two equilibrium configurations: low density and high density. This procedure generates models that are analytically and computationally tractable and that one hopes are capable of retaining the qualitative features of the real complex systems. The physical motivation behind these studies is the assumption that two length scales systems exhibit the same anomalous behaviors present in water.

Confirming this hypothesis a number of continuous [1, 2, 4–7] and lattice gas models [8–16] show the presence of density, diffusion and structural anomalous behavior as observed in water [17, 18].

In addition to the seventy-two anomalies [19], water has at very low temperatures two coexisting amorphous phases with distinct densities: the low density amorphous (LDA) and high density amorphous phases (HDA) [20–24]. These two amorphous phases led to the hypothesis of the existence at higher temperatures of two liquid phases: a low density liquid and high density liquid phases. Such conjecture establishes that the coexistence between these two liquid phases ends in a second critical point or also called, liquid-liquid critical point (LLCP) [24]. Experiments for testing the existence of this criticality are difficult since the region in the pressure versus temperature phase diagram where the alleged critical point exists is locate beyond the homogeneous nucleation limit. In order to circumvent this difficulty for testing the existence of the liquid-liquid critical point recently confined geometries have been employed [25, 26]. In these nanoconfined geometries the disruption of the hydrogen bonds suppress the solidification of the system and allows for maintaining the system liquid in temperatures in which otherwise would be solid [25, 26]. These experimental systems show convincing evidences that water exhibits two liquid structures at low temperatures.

The use of confining water, however brings another set of issues. What guarantees that the same thermodynamic and dynamic anomalies and criticality present in the bulk are not destroyed as the system is confined? Can confinement bring up new phenomena not

present in the bulk system? In order to answer these questions water-like atomistic or continuous effective potential models were explored confined by different geometries such as plates [27–33], one pore [34–42] and disordered matrix [39, 48–52]. These simulations show that confinement leads to a controversial result regarding the melting line. While results for SPC/E water show that the melting temperature for hydrophobic plates is lower than the bulk and higher than for hydrophilic walls, for mW model no difference between the melting temperature due to the hydrophobicity [43] is found.

In confined systems the TMD occurs at lower temperatures for hydrophobic confinement [44, 45] and at higher temperatures for hydrophilic confinement [46] when compared with the bulk. The diffusion coefficient, D, in the direction parallel to the plates exhibit an anomalous behavior as observed in bulk water. However the temperatures of the maximum and minimum of D are lower than in bulk water [45]. In the direction perpendicular to the plates, no diffusion anomalous behavior is observed [47].

In addition to the usual density and diffusion anomalous behavior, these confined systems show a variety of new effects not present in the bulk. For example, fluids confined in carbon nanotube exhibit formation of layers, crystallization of the contact layer [53, 54] and a superflow not present in macroscopic confinement [55, 56].

The confinement by a pore, within plates or nanotubes is symmetric and even though it introduces a breaking of the water hydrogen bond network, this is done in an ordered way. Confining matrix such as the ones present in plants and underground water are not ordered. Recently the effects of an water-like liquid confined in a disordered matrix have been analyzed using a model in which the bonds are introduced by the inclusion of Potts variables [49]. This study shows that the liquid-liquid coexistence line is affected by the increase of the density of random porous in the matrix without disappearing.

In all these studies, however the liquid-liquid transition is preserved and the density of confining matrix is not very high. Here, we give a further step by investigating effects imposed by disordered porous when the random matrix exhibits a high density. The system is defined in a triangular lattice where the obstacles are fixed and randomly distributed. The fluid is modeled as a Associating Lattice Gas Model [12] defined an occupational variable together with a bond orientational variable. This model in the bulk shows the density and diffusion anomalies present in water and the liquid-gas and liquid-liquid criticality [12]. Here we explore the effect in the chemical potential versus temperature phase diagram of

the presence of the random fixed obstacles.

This paper is organized as following. In Sec. II we present the model used here. In Sec. III outline details of Monte Carlo simulations and how was calculated the thermodynamic properties of system. Results are presented in Sec. IV, followed by conclusions in Sec. V.

II. THE MODEL

The model system is defined in a triangular lattice. Each accessible site i can be empty or occupied by a water molecule. Empty sites have $\sigma_i = 0$ while occupied sites have $\sigma_i = 1$. Each water molecule has orientational states represented by the variable τ that presents six arms, being two inert arms with $\tau_i = 0$ and four active arms with $\tau_i = 1$. They represent the possibility of a molecule to form hydrogen bonds with up to four neighbor molecules. For representing the symmetry present in water, two inert arms are diametrically positioned and just three different orientational states are possible. Fig. 1 exemplifies the geometry of a water molecule. A hydrogen bond is formed only when the active arms of two neighbor

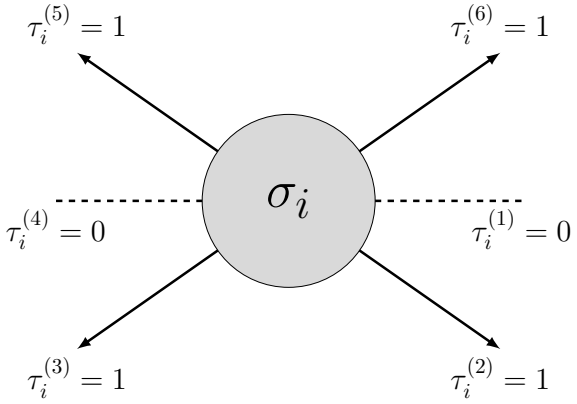


FIG. 1. The occupational and orientational states of a water molecule placed at the site i. In such example, the arms variables of molecule read: $\tau_i^{(1)} = 0$, $\tau_i^{(2)} = 1$, $\tau_i^{(3)} = 1$, $\tau_i^{(4)} = 0$, $\tau_i^{(5)} = 1$, $\tau_i^{(6)} = 1$.

molecules point out to each other, $\tau_i \tau_j = 1$. In this case, the interaction energy between two bonded arms reads $-v$ and while non bonded arms contribute with a higher energy of $-v + 2u$ (punishement for non forming hydrogen bonds). The Hamiltonian of the system is

given by

$$\mathcal{H} = 2u \sum_{\langle i,j \rangle} \sigma_i \sigma_j \left[\left(1 - \frac{v}{2u} \right) - \tau_i \tau_j \right] - \mu \sum_i \sigma_i. \quad (1)$$

The phase behavior of the system in the absence of obstacles was already analyzed [15]. Below it will be reviewed. At ground state, $T^* \equiv T/v = 0$, the grand potential per site is $\Phi = e - \mu N$ where $e = \langle \mathcal{H} \rangle / L^2$. For low chemical potentials, the lattice is empty and the system is constrained in gas phase, $\rho = 0$. In this phase the grand potential is $\Phi_{GAS} = 0$. Increasing the chemical potential the system reaches a point at which the gas phase coexists with a low density liquid phase (LDL). In this phase, the density is $\rho = 3/4$ and each particle forms four hydrogen bonds with its neighbor, resulting in a grand potential per site $\Phi_{LDL}/L^2 = -(3/2)v - (3/4)\mu$ and consequently in a gas-LDL coexistence chemical potential $\mu^*_{G-LDL} = \mu_{G-LDL}/v = -2$. For high chemical potentials, all sites of lattice are occupied by particles, resulting in a density $\rho = 1$ and grand potential per site $\Phi_{HDL}/L^2 = -3v + 2u - \mu$. The coexistence between the LDL phase and the HDL phase occurs at $\mu^*_{LDL-HDL} = \mu_{LDL-HDL}/v = 8u/v - 6$. The main features of LDL and HDL phases are exemplified in Fig. 2 for two possible configurations at $T^* = 0$. At temperatures

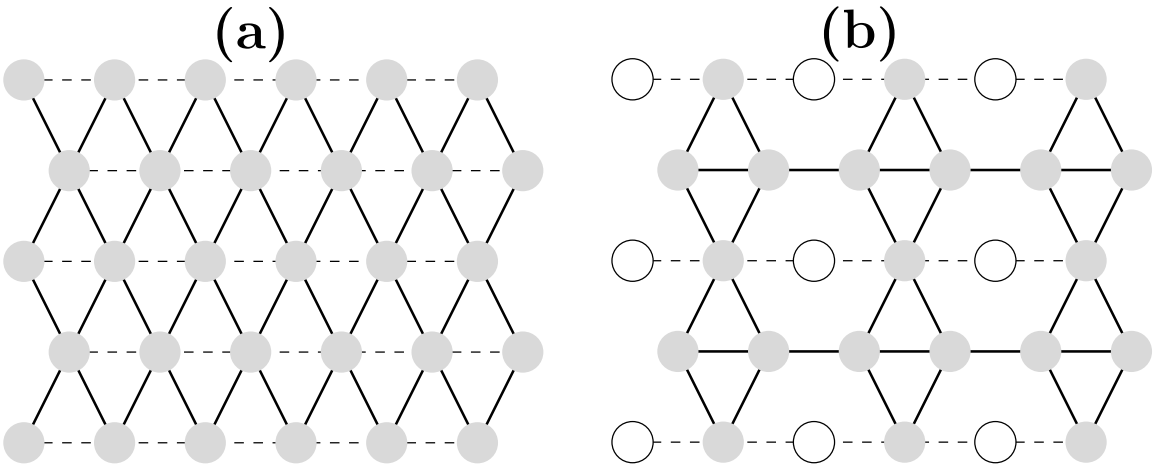


FIG. 2. (a) HDL phase for the bulk system. The solid lines indicate the bonding arms (b) LDL phase for the bulk system. The solid lines indicate the bonding arms.

$T^* > 0$, the model was studied by Monte Carlo simulations whose phase diagram is shown in Fig. 3. The gas-LDL and LDL-HDL transition lines are first-order transitions, ending in respective tricritical points T_{c1} and T_{c2}, respectively that are joined by a line of continuous transitions, called $\lambda-$line. For the bulk case, T_{c1} and T_{c2} read 0.65 and 0.825, respectively.

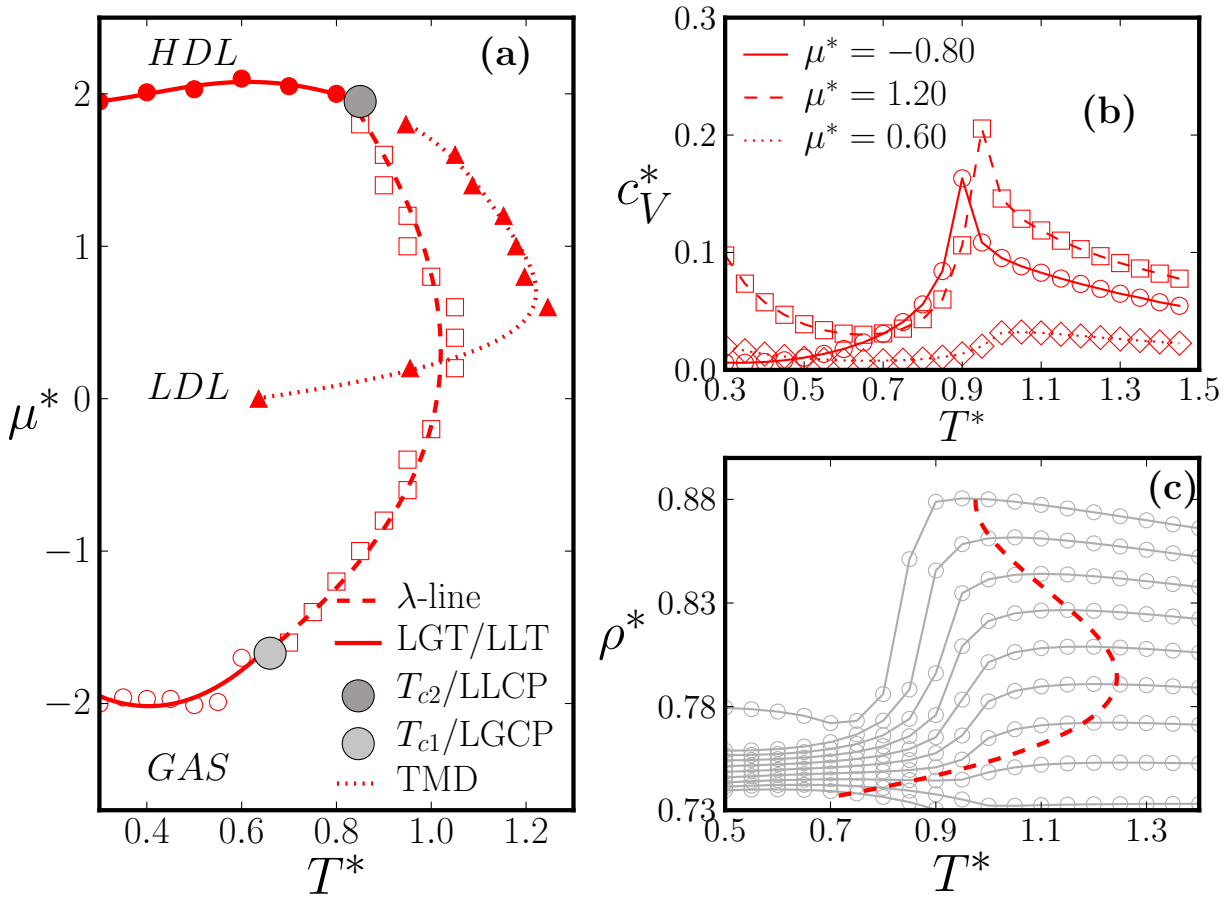


FIG. 3. For the bulk System, panel (a) shows the phase diagram μ^* vs T^*, illustrating the gas-LDL (empty circles) and the LDL-HDL (filled circles) phase transitions, the λ-line (empty squares) and the TMD line (filled triangles). In panel (b) we plot the c_V^* versus T^* for $\mu^* = -0.80$ (circles), $\mu^* = 0.60$ (diamonds) and $\mu^* = 1.20$ (squares). In (c) the system density ρ versus T^* for fixed μ^*along the TMD line (dashed line).

In order to understand the differences between the LDL and HDL phases, we divide the lattice in four sublattices as illustrated in the Fig. 4. The LDL phase is characterized by one of the sublattices being empty while all the others are filled, in such a way that the transition to the HDL phase occurs when the empty sublattice is filled. Also, it is signed by a rotation in the inert arms, in which in the HDL phase they are all parallel. In addition, in the LDL phase each particle forms four bonded arms that show a zigzag structure, whereas in the HDL phase each particle also forms four bonded arms but in addition to the zigzag structure two parallel lines appear. In the regime of very high temperatures, the system is

disordered, in which the sublattice occupations do not exhibit any ordering. By lowering T, the λ-line is crossed, which one sublattice is emptied and the others remaining filled with an reorganization of the inert arms that form the above ordered zig-zag structure.

The density of bonds, $\rho_{hb} = \frac{1}{L^2}\sum_{i=1}^{L^2}\sum_{i+\delta}\sigma_i\sigma_{i+\delta}\tau_i\tau_{i+\delta}$ is also an important quantity for characterizing the phase transitions. At $T^* = 0$ the gas, LDL and HDL phases has ρ_{hb} reading $0, 1.5$ and 2, respectively. Thus the phase transitions are also signed by changes in the fraction of hydrogen bonds. At high temperature the system is disordered and the $\lambda-$line is obtained through the specific heat at constant volume c_V by

$$c_V = \frac{1}{VT^2}\left[\left\langle \delta\mathcal{H}^2\right\rangle_{\text{gcan}} - \frac{\left\langle \delta\mathcal{H}\delta N\right\rangle^2_{\text{gcan}}}{\left\langle \delta N^2\right\rangle_{\text{gcan}}}\right] + \frac{3Nk_B}{2V} \tag{2}$$

where $\delta X = X - \langle X\rangle$ with $X = \mathcal{H}$ and N and averages are evaluated in the ensemble of T, μ fixed.

In this work the porous matrix is introduced by considering fixed obstacles that are randomly distributed in the lattice. Each obstacle occupies a single site and interacts with the particles via a "hard core" constraint. The density of obstacles is given by $\rho_o = N_o/L^2$ where N_o is the number of obstacles and L^2 is the system volume. In Fig. 4, we exemplify a lattice configuration composed of water, obstacles and empty sites.

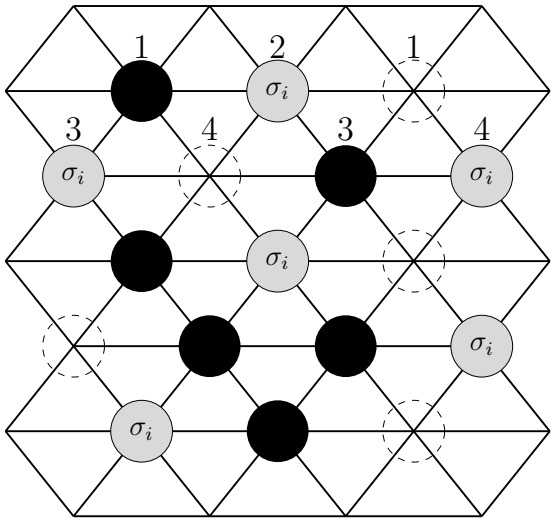


FIG. 4. Example of a lattice configuration. Gray, black and dashed circles describes water molecules, obstacles and empty sites, respectively. For clarity, hydrogen bonds have not explicitly shown.

III. THE METHODS AND SIMULATION DETAILS

All the thermodynamic properties have been obtained by performing grand canonical Monte Carlo (MC) simulations for fixed T^*, μ^* and ρ_0 [57]. Microscopic configurations are generated according to the Metropolis algorithm [58] described as follows. Obstacles are initially randomly distributed and a given site k other than a porous is randomly chosen. Two sorts of transitions are possible, taking into account k be empty or occupied by a water molecule. In the former case, a water molecule in one of its arm states is chosen, whereas in the latter one of the three possibilities (including the other two arm states and empty site) are performed. All of possible transitions are chosen with equal probability. Next, we evaluate the energy difference $\Delta\mathcal{H}$ between the original and the new configuration. The configuration change is accepted according to the Metropolis prescription $\min\{1, e^{-\beta\Delta\mathcal{H}}\}$, where $\beta = 1/k_BT$. A Monte Carlo step is defined as the number of trials for generating new configurations. After discarding a sufficient number of initial MC steps, relevant quantities are evaluated. In addition to the thermodynamic quantities, we also investigated the influence of obstacles in the dynamic properties, characterized through the diffusion coefficient D given by Einstein's relation

$$D = \lim_{t\to\infty} \frac{\langle \Delta r(t)^2 \rangle}{4t}, \tag{3}$$

where $\langle \Delta r(t)^2 \rangle = \langle (r(t) - r(0))^2 \rangle$ is the mean square displacement per particle and time is measured in Monte Carlo steps. The numerical MC procedure for calculating the diffusion is described as follows. First, the system is equilibrated by employing the previous Metropolis dynamics for fixed T^* and μ^*. After the equilibrium is reached, an occupied site i and it's neighbor j are chosen randomly. In case of neighbor site j be empty, the molecule moves to the empty site also following the above Metropolis prescription $\min\{1, e^{-\beta\Delta\mathcal{H}}\}$, where $\Delta\mathcal{H}$ is the difference of energy due to the movement. A Monte Carlo step is defined through the number of trials of movement for every particle. After repeating this algorithm nt times, where n is the number of molecules in the lattice, the diffusion coefficient is calculated from Eq.(3).

Numerical simulations have been performed for triangular lattices of size $L = 35$ and periodic boundary conditions for three representative values of density of obstacles $\rho_o = 0.08, 0.24$ and 0.40 have been considered. In all cases, we have used 10^6 Monte Carlo (MC) steps to equilibrate the system and 10^6 MC steps for evaluating the relevant quantities.

IV. RESULTS

A. Structural and thermodynamic behavior

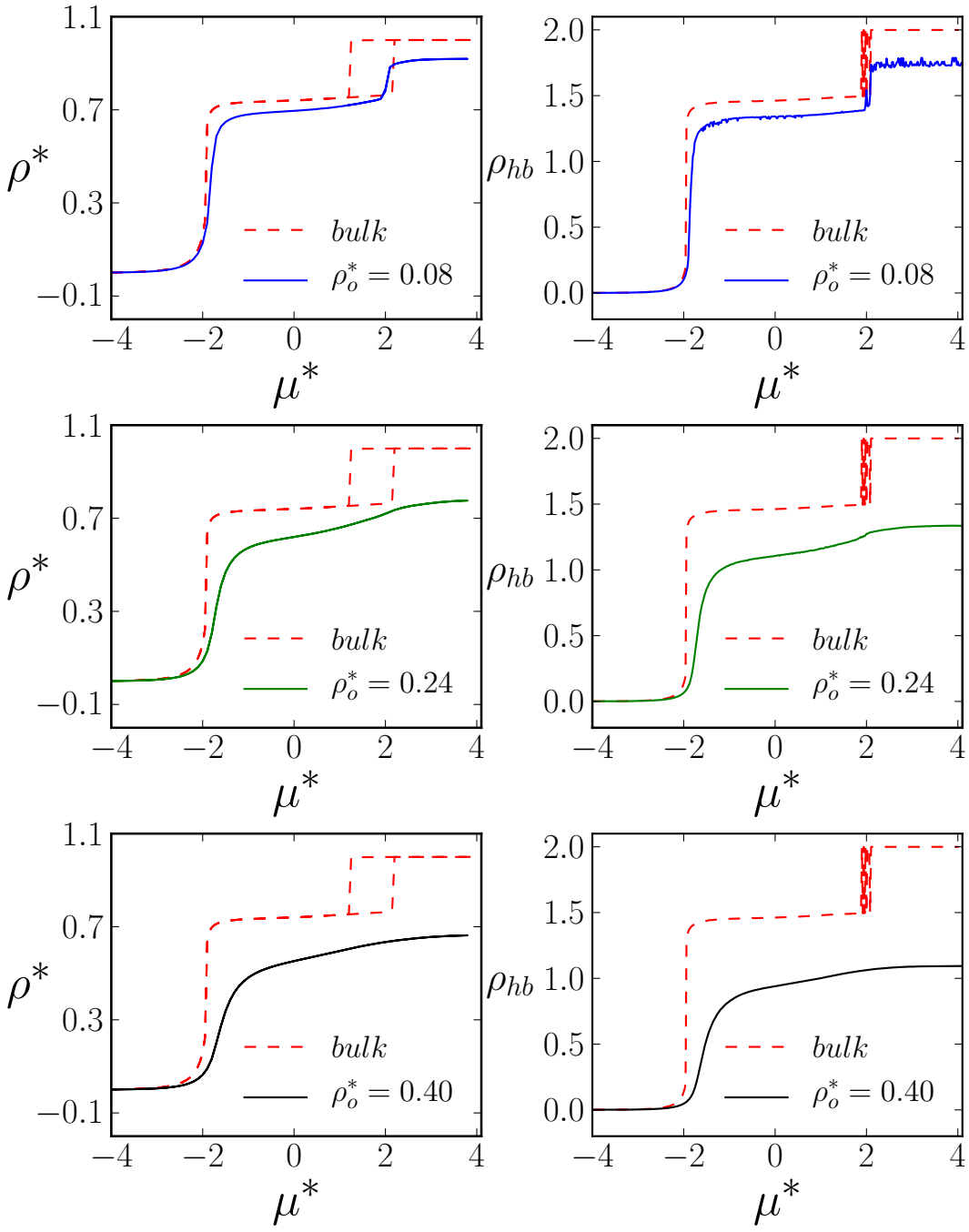


FIG. 5. ρ vs μ^* for distinct porous densities ρ_o for $T^* = 0.40$.

First, let us exam what happens with the phases present in the bulk system as the

obstacles are introduced. Fig. 5 shows the water density ρ, versus the reduced chemical potential μ^*, for distinct porous densities at the fixed temperature $T^* = 0.40$. The inclusion of obstacles changes the gas-LDL and the LDL-HDL phase transition, whose effect becomes more pronounced as ρ_o increases. In particular, by raising the porosity, the density gap between the liquid phases becomes less abrupt and inclusion of obstacles move the transition points for larger chemical potentials. Figs. 6, 7 and 8 illustrate the chemical potential versus temperature phase diagrams for $\rho_o = 0.08, 0.24$ and 0.40, respectively. In particular, by increasing ρ_o the tricritical points T_{c1} and T_{c2}, in which the gas-LDL and LDL-HDL coexistence lines meet the $\lambda-$line, decreases as shown in Figs. 6 , 7 and 8. More specifically, while the bulk gas-LDL tricritical point is located at $T_{c1} = 0.65$, it moves to $T_{c1} = 0.60, 0.55$ and 0.52 for $\rho_o = 0.08, 0.24$ and 0.40, respectively.

This scenario becomes even more drastic in the case of the LDL-HDL phase transition. The tricritical point not only decreases its value from $T_{c2} = 0.825$ (bulk) to $T_{c2} = 0.57$ and $T_{c2} = 0.52$ for $\rho_o = 0.08$ and 0.24, respectively but it disappears for $\rho_o = 0.40$, implying the absence of liquid-liquid transition line. In addition the λ-line can also be found only for $\rho_o = 0.08, 0.24$, in which for $\rho_0 = 0.40$ the original bulk tricritical T_{C1} becomes a single critical point .

The above changes in liquid phases as well as transition points can be understood by verifying that the inclusion of porous suppress partially the structured patterns found in the LDL and HDL phases (see e.g Fig. 2(a) and (b) for the bulk case). In the case of the LDL phase the ordered bulk structure is distorted as ρ_0 increases, as illustrated in the Fig. 9 for $\mu^* = -0.5$. For the lowest case $\rho_o = 0.08$, the degree of confinement is low and most occupied sites preserve at least three bonds. As the density of obstacles is increased (here exemplified for $\rho_o = 0.16$ and 0.24) the fraction of disrupted bonds increases, reaching a limit in which the connectivity of the network is lost. Similar effect is verified in the HDL phase, but the effect is more pronounced in such case. This can be understood by recalling that in contrast to the HDL phase, porous occupy partially empty sites with neighboring molecules not forming hydrogen bonds in the LDL phase. This lost of connectivity also explains, in similarity with the decrease of tricritical points, why the transition from the disordered structure to the LDL through the λ-line occurs for lower temperatures than the bulk. Recalling that such transition is characterized by the disordered phase ordering by making one of the sublattices empty, the inclusion of porous makes the system entropy

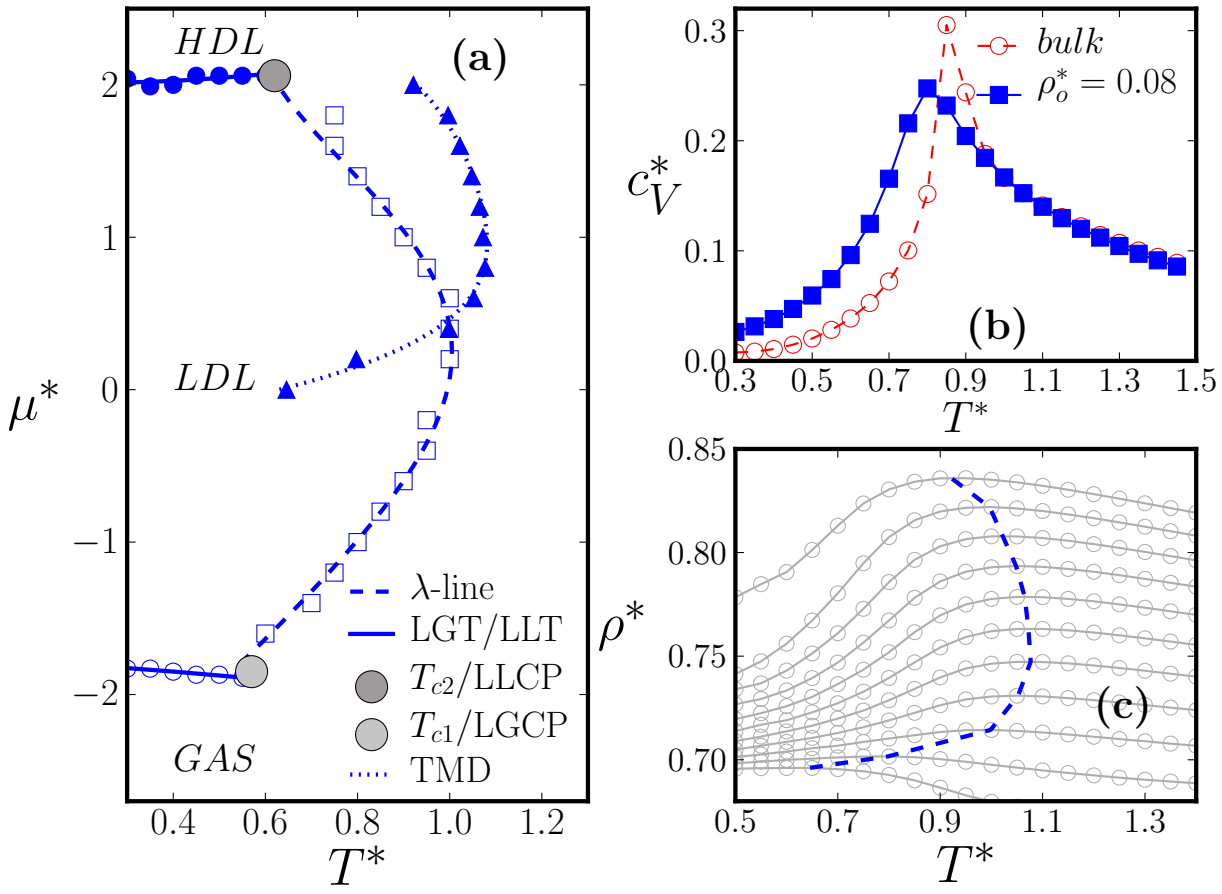


FIG. 6. For $\rho_o = 0.08$, in (a) the phase diagram in the plane of reduced chemical potential μ^* versus reduced temperature T^*. Empty and filled circles denote the Gas-LDL and the LDL-HDL phase transitions, respectively. The λ and TMD lines are described by empty squares filled triangles, respectively. Panel (b) shows the specific heat at constant volume c_V versus T^* for the system with obstacles (filled squares) and bulk system (empty circles) at $\mu = -1.00$. Panel (c) shows ρ versus T^* for $\mu^* = 0.0, \ldots, 2.2$ showing the TMD line (dashed line).

be larger than the bulk, with partial disruption of hydrogen bonds. Thus, all transition points, move for lower temperatures as a way for "compensating" the above increase of disorder. In other words, due to the inclusion of porous, the structured phases exist only for lower temperatures than the bulk, whose decreasing become more pronounced as ρ_0 increases. Finally, for high density of obstacles the transition is destroyed by enhancement of fluctuations. The last comment concerns in the comparison between the TMD as ρ_0 increases. As for the transition lines, the TMD shortens and move for lower temperatures

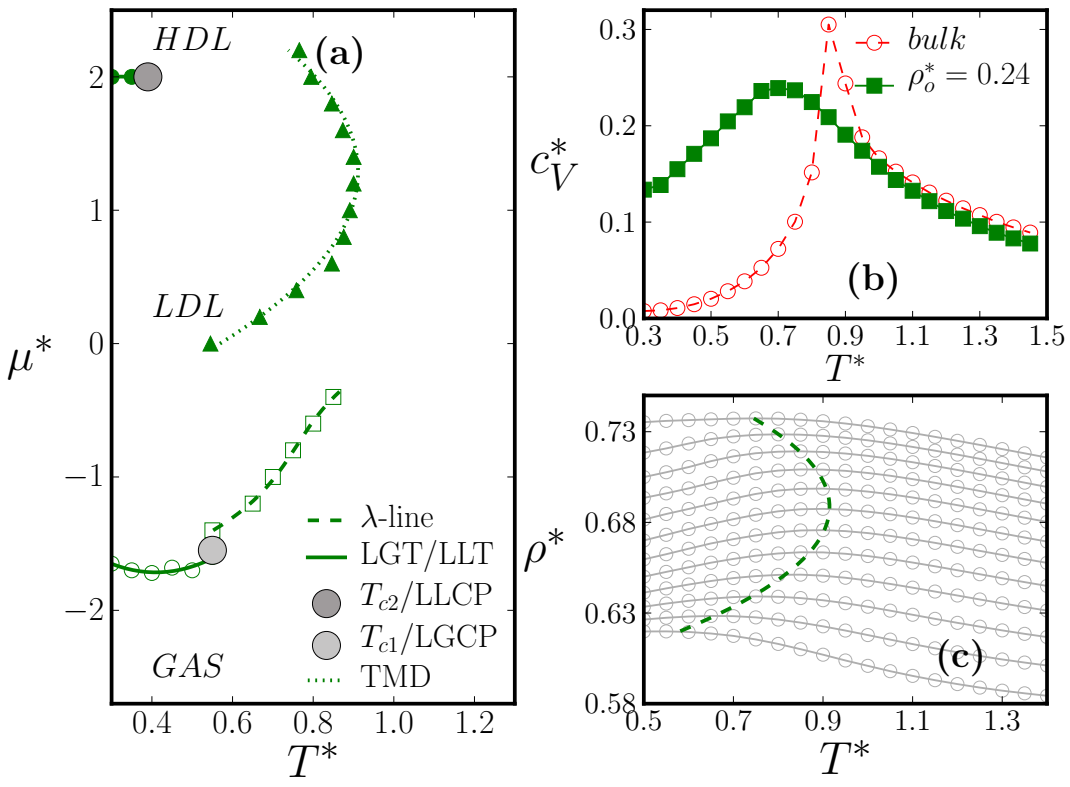


FIG. 7. For $\rho_o = 0.24$, in (a) the phase diagram in the plane of reduced chemical potential μ^* versus reduced temperature T^*. Empty and filled circles denote the Gas-LDL and the LDL-HDL phase transitions, respectively. The λ and TMD lines are described by empty squares filled triangles, respectively. Panel (b) shows the specific heat at constant volume c_V versus T^* for the system with obstacles (filled squares) and bulk system (empty circles) at $\mu = -1.00$. Panel (c) shows ρ versus T^* for $\mu^* = 0.0, \ldots, 2.0$ showing the TMD line (dashed line).

(with maximum ρ decreasing) as ρ_0 increases. However, in contrast previous results, for $\rho_0 = 0.40$ a tiny TMD (ranged from $T^* = 0.50$ to 0.70 with $\rho = 0.56$ to 0.64) is verified.

B. Diffusion and dynamic anomaly

Besides the influence of immobile obstacles in the thermodynamic quantities, another relevant question concerns what happens with the system mobility as the density of obstacles increases. Fig. 11 shows the diffusion coefficient computed using Eq. (3) for different T^*'s and ρ_0's. In similarity with the pure model, the diffusion coefficient presents an increasing anomalous behavior until a maximum value by raising ρ for $\rho_0 = 0.08$ and 0.24. The only

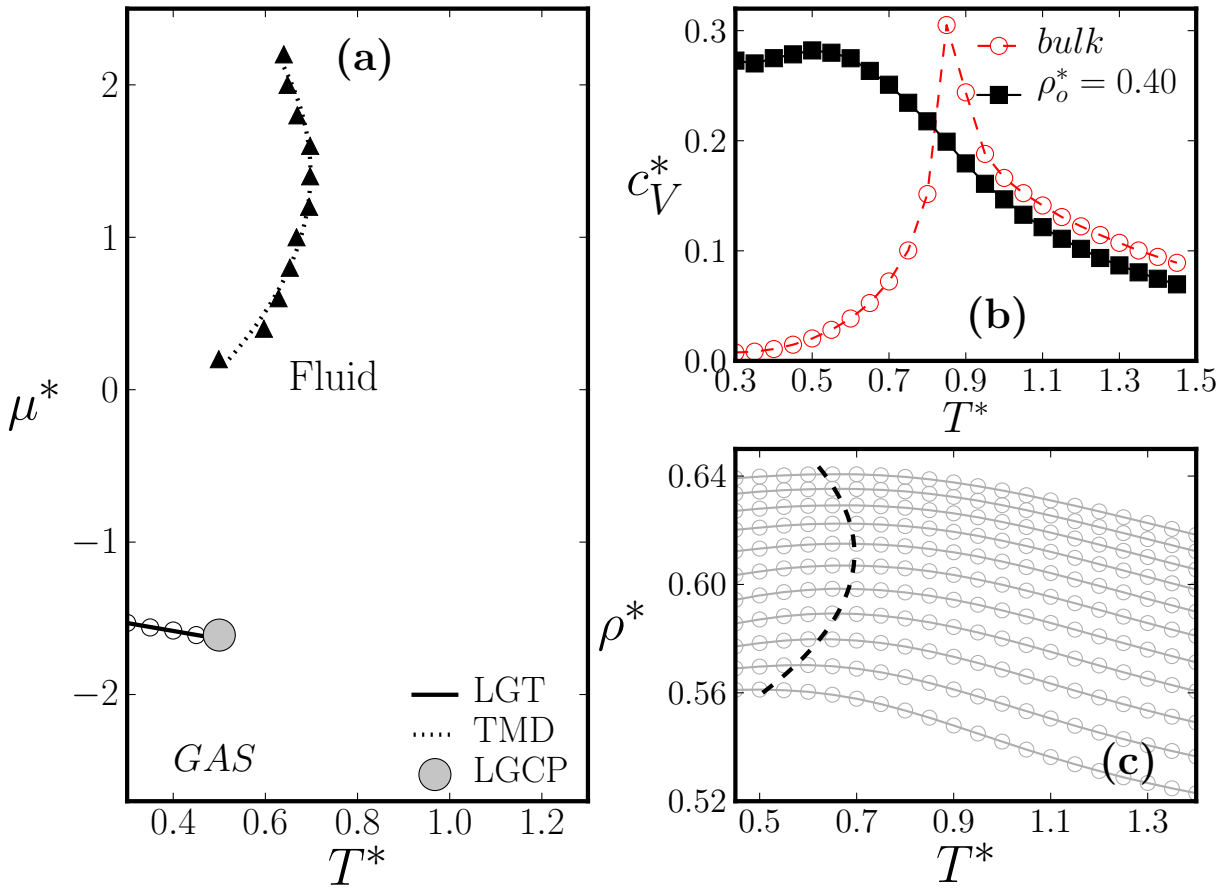


FIG. 8. For $\rho_o = 0.40$, in (a) the phase diagram in the plane of reduced chemical potential μ^* versus reduced temperature T^*. Empty and filled circles denote the Gas-LDL and the LDL-HDL phase transitions, respectively. The λ and TMD lines are described by empty squares filled triangles, respectively. Panel (b) shows the specific heat at constant volume c_V versus T^* for the system with obstacles (filled squares) and bulk system (empty circles) at $\mu = -1.00$. Panel (c) shows ρ versus T^* for $\mu^* = 0.2, \ldots, 2.2$ showing the TMD line (dashed line).

exception is the case with density of obstacles 0.40.

The reason concerns that the dynamic anomaly depends crucially of the presence of a high number of neighbor sites occupied by the fluid [62]. The obstacles make this difficult and for a very high number of obstacles, the mobility becomes even impossible.

Since for water-like systems, typically the region in the μ^*-T^* phase diagram in which the density anomaly is present is close to the region where the diffusion anomaly appears. Therefore one expects that the suppression of the first is directly related to the disappearance

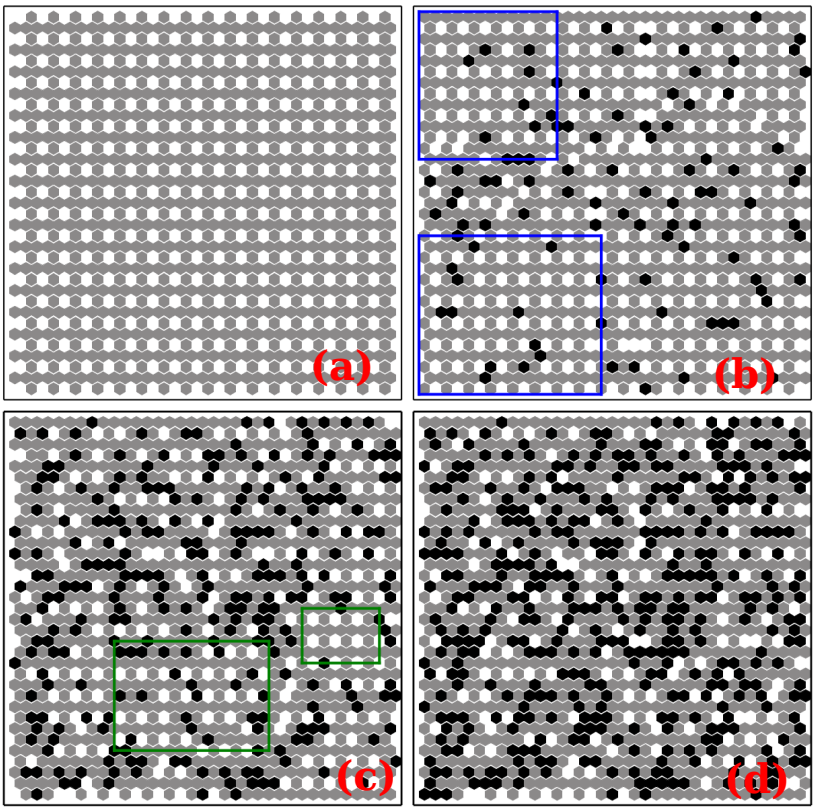


FIG. 9. Spatial snapshot (35 × 35 sites) of triangular lattice. Each site is represented by hexagon, with its six nearest-neighbor sites. White hexagons represent vacancies, black represent obstacles and gray represent water-like particles. The snapshots exhibit character configurations of system with chemical potential $\mu^* = -0.5$ and temperature $T^* = 0.3$. In (a) we present the bulk system. In (b) the system submitted at low degree of confinement $\rho_o = 0.08$ and the blue rectangles denote the regions where the characteristic geometry of LDL of ALG is preserved. In (c), intermediate degree of confinement $\rho = 0.24$, and green rectangles denote the LDL structure. The highest degree of confinement $\rho = 0.40$ is shown in (d).

of the other.

V. CONCLUSION

The effects of fixed obstacles in thermodynamic and dynamic properties of an simplified water-like model have been investigated. For low degree of confinement, the thermodynamic, structural and dynamic properties of model are almost totally preserved due to the low steric

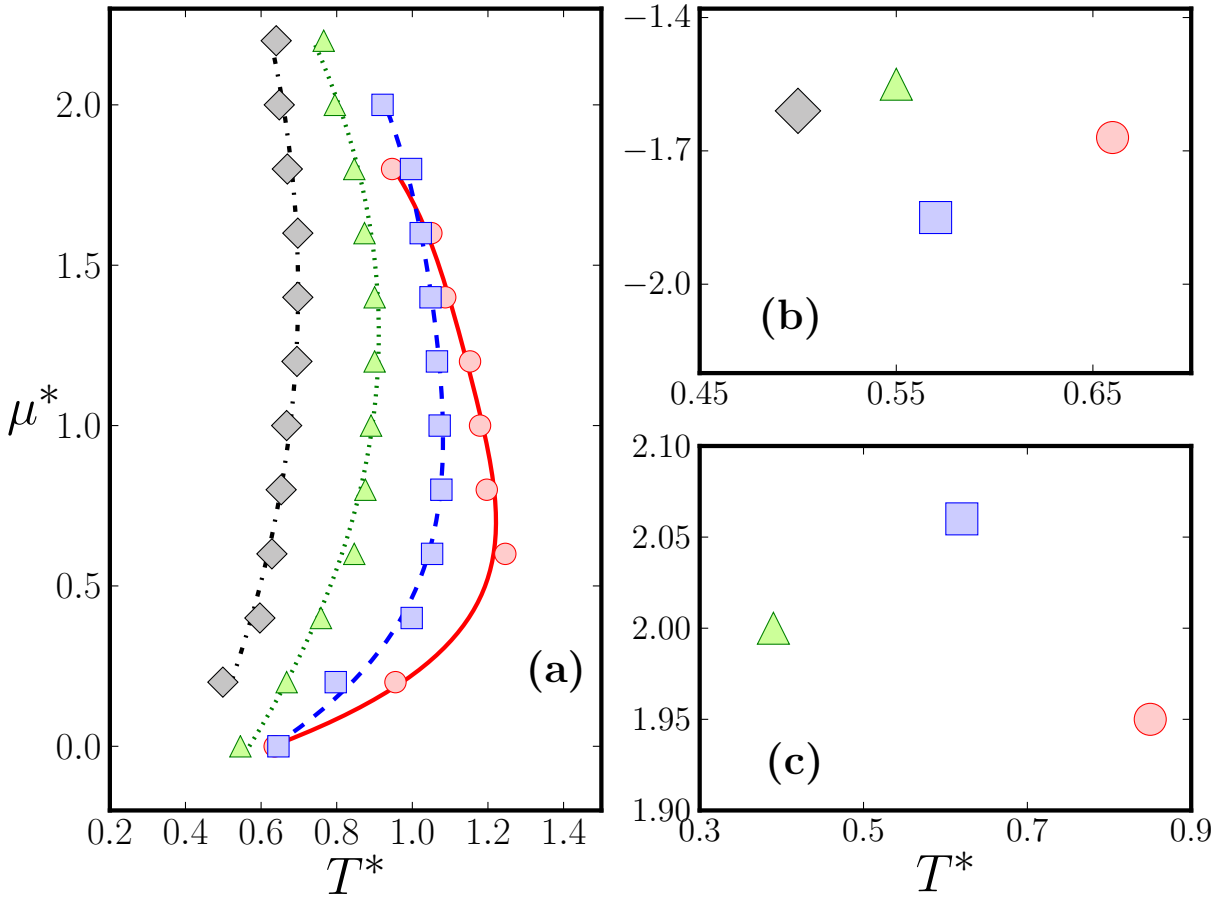


FIG. 10. Chemical potential versus temperature illustrating (a) the TMD lines (b) the gas-LDL tricritial point (c) the LDL-HDL critical point values for the bulk and the system with different concentrations of obstacles.

effects. For intermediate case, $\rho_o = 0.24$, the system suffers significant changes such as, the decrease of the critical and tricritical points to lower temperatures, resulting in a reduction of coexistence regions. This effect is more dramatic for the liquid-liquid coexistence that disappear for $\rho_o = 0.40$. The density and diffusion anomalous regions are also shifted to lower temperature, keeping the reduction in temperature-chemical potential phase diagram. The disappearance of the liquid-liquid temperature also reflects in the absence of density and diffusion anomalous regions in the limit of large density of obstacles. Both effects are related to both the entropy increase due to the presence of the obstacles and the disruption of the bonds network.

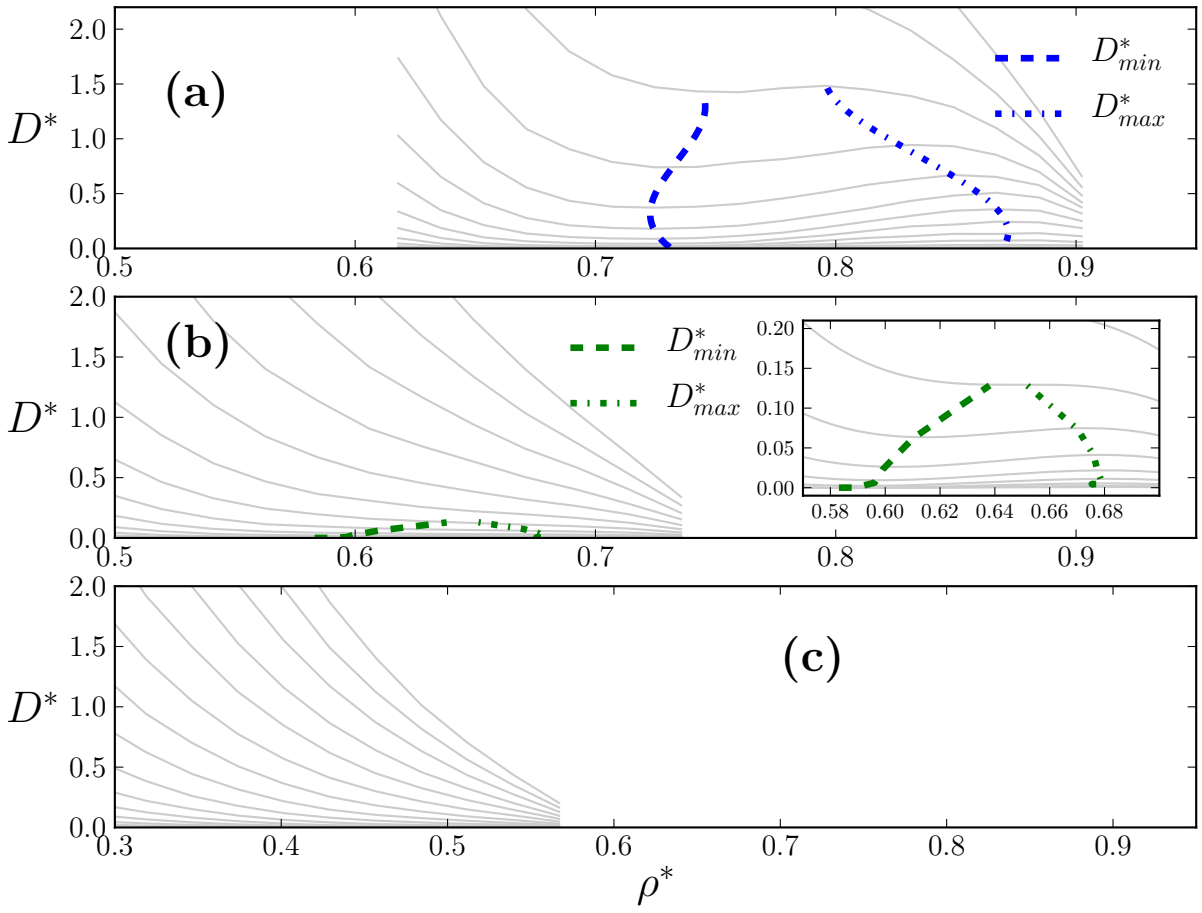


FIG. 11. Diffusion coefficient versus density at fixed temperature. The gray lines are fit of diffusion obtained by simulation. In case (A) we present the results for $\rho_o = 0.08$, in which the gray lines are just fit of diffusion obtained by simulation , blue dashed and dot-dashed connect the minimum and maximum in diffusion respectively. In (B) we have the same plot of case (A) but for the case $\rho_o = 0.24$ and on inset we plot a zoom of anomalous region. In (C) the results for $\rho_o = 0.40$. The temperatures studied were $T^* = 0.30 \ldots 1.00$ with $\Delta T^* = 0.05$

VI. ACKNOWLEDGMENTS

We acknowledge the Brazilian agency CAPES (Coordenação de Aperfeiçoamento de Pessoal de Nível Superior) for the financial support and Centro de Física Computacional - CFCIF (IF-UFRGS) for computational support .

[1] P. C. Hemmer, G. Stell, Phys. Rev. Lett. **24**, 1284 (1970).

[2] P. G. Debenedetti P G, V. S. Raghavan, S. S. Borick, J. Phys. Chem. **95**, 4540 (1991).

[3] C. H. Cho, S. Singh, G. W. Robinson, Phys. Rev. Lett. **76**, 1651 (1996).

[4] E. A. Jagla, Phys. Rev. E **58**, 1478 (1998).

[5] P. Camp, Phys. Rev. E **68**, 061506 (2003).

[6] A. B. de Oliveira, P. A. Netz, T. Colla, M. C. Barbosa, J. Chem. Phys. **124**, 084505 (2006).

[7] Y. D. Fomin, N. V. Gribova, V. N. Ryzhov, S. M. Stishov, D. Frenkel, J. Chem. Phys. **129**, 064512 (2008).

[8] G. M. Bell, D. A. Lavis, J. Phys. A **3**, 568 (1970).

[9] D. A. Lavis, J. Phys. C **6**, 1530 (1973).

[10] G. Franzese, H. E. Stanley, J. Phys.: Condens. Matter **14** ,2201 (2002).

[11] C. Buzano, M. Pretti, J. Chem. Phys. **119**, 3791 (2003).

[12] V. B. Henriques, M. C. Barbosa, Phys. Rev. E **71**, 031504 (2005).

[13] V. B. Henriques, N. Guissoni, M. A. Barbosa, M. Thielo, M. C. Barbosa, Mol. Phys. **103**, 3001 (2005).

[14] N. G. Almarza, J. A. Capitan, J. A. Cuesta, E. Lomba, J. Chem. Phys. **131** 124506 (2009).

[15] A. L. Balladares, V. B. Henriques, M. C. Barbosa, J. Phys.: Condens. Matter **19**, 116105 (2007).

[16] M. Szortyka, M. Girardi, V. B. Henriques, M. C. Barbosa, J. Chem. Phys. **130**, 184902 (2009).

[17] G. S. Kell, Nature **20**, 97 (1975).

[18] C. A. Angell, E. D. Finch, P. Bach, J. Chem. Phys. **65** , 3063 (1976).

[19] Martin Chaplin, Seventy-two anomalies of water, http://www.lsbu.ac.uk/water

[20] O. Mishima, Phys. Rev. Lett. **85**, 334 (2000).

[21] O. Mishima, Chem. Phys. Lett. **422** 507 (2006).

[22] P. H. Poole, F. Sciortino, E. Ulrich, H. E. Stanley, Phys. Rev. E **48**, 3799 (1993).

[23] Osamu Mishima, J. Chem. Phys. **100**, 5910 (1994).

[24] P H. Poole, F. Sciortino, E. Ulrich, H. E. Stanley, Nature **360**, 324 (1992).

[25] L. Xu, P. Kumar, S. V. Buldyrev, S. -H. Chen, P. Poole, F. Sciortino, H. E. Stanley, Proc. Natl. Acad. Sci. USA **102**, 16558 (2005).

[26] S. -H. Chen, F. Mallamace, C. Y. Mou, M. Broccio, C. Corsaro, A. Faraone, L. Liu, Proc. Natl. Acad. Sci. USA **103**, 12974(2006).

[27] J. R. Bordin, L. B. Krott, M. C. Barbosa, J. Phys. Chem. C **118**, 9497 (2014).

[28] Leandro B. Krott, Marcia C. Barbosa, Phys. Rev. E **89**, 012110 (2014).

[29] Leandro B. Krott, Marcia C. Barbosa, J. Chem. Phys. **138**, 084505 (2013).

[30] P. Kumar, S. V. Buldyrev, F. W. Starr, N. Giovambattista, H. E. Stanley, Phys. Rev. E **72**, 051503 (2005).

[31] P. Scheidler, W. Kob, K. Binder, Europhys. Lett. **59**, 701 (2002).

[32] M. Meyer, and H. E. Stanley, J. Phys. Chem. B **103**, 9728 (1999).

[33] N. Giovambattista, P. J. Rossky, P. G. Debenedetti, Phys. Rev. Lett. **102**, 050603 (2009).

[34] J. R. Bordin, J. S. Andrade Jr., A. Diehl, M. C. Barbosa, J. Chem. Phys. **140**, 194505 (2014).

[35] R. Bordin, Alexandre Diehl, Marcia C. Barbosa, J. Phys. Chem. B **117**, 7047 (2013).

[36] R. Bordin, A. B. de Oliveira, A. Diehl, Marcia C. Barbosa, J. Phys. Chem. B **137**, 084504 (2012).

[37] R. Bordin, A. Diehl, M. C. Barbosa, Y. Levin, Phys. Rev. E **85**, 031914 (2012).

[38] D. Corradini, P. Gallo, M. Rovere, J. Mol. Liq. **159**, 18 (2011).

[39] P. Gallo, M. Rovere, Phys. Rev. E **76**, 061202 (2007).

[40] P. Gallo, M. Rapinesi, M. Rovere, J. Chem. Phys. **117**, 369 (2002).

[41] P. Gallo, M. Rovere, S-H. Chen, J. Phys. Chem. Lett. **1**, 729 (2010).

[42] P. Gallo, M. Rovere, S-H. Chen, J. Phys.: Condens. Matter **24**, 064109 (2012).

[43] E. B. Moore, J. T. Allen, and V. Molinero, J. Phys. Chem. C **116**, 7507 (2012).

[44] N. Giovambattista, P. J. Rossky, and P. G. Debenedetti, Phys. Rev. Lett. **102**, 050603 (2009).

[45] P. Kumar, S. V. Buldyrev, F. W. Starr, N. Giovambattista, and H. E. Stanley, Phys. Rev. E **72**, 051503 (2005).

[46] S. R.-V. Castrillon, N. Giovambattista, I. A. Aksay, and P. G. Debenedetti, J. Chem. Phys. B **113**, 1438 (2009).

[47] S. Han, P. Kumar, and H. E. Stanley, Phys. Rev. E **77**, 030201 (2008).

[48] E. G. Strekalova, M. G. Mazza, H. E. Stanley, G. Franzese, J. Phys.: Condens. Matter **24**, 064111 (2012).

[49] E. G. Strekalova, J. Luo, H. E. Stanley,G. Franzese, S. V. Buldyrev, Phys. Rev. Lett **109**, 105701 (2012).

[50] P. A. Bonnaud, B. Coasne, R. J.-M. Pellenq, J. Phys.: Condens. Matter **22**, 284110 (2010).

[51] O. Pizio, H. Dominguez, L. Pusztai, S. Sokolowski, Physica A **338**, 2278 (2009).

[52] K. S. Page, P. A. Monson, Phys. Rev. E **54**, 6557 (1996).

[53] S. T. Cui, P. T. Cummings, H. D. Cochran, J. Chem. Phys. **114**, 7189 (2001).

[54] A. Jabbarzadeh, P. Harrowell, R. I. Tanner, J. Chem. Phys. **125**, 034703 (2006).

[55] H. Chen, J. K. Johnson, D. S. Sholl, J. Phys. Chem. B **110**, 1971 (2006).

[56] X. Qin, Q. Yuan, Y. Zhao, S. Xie, Z. J. Liu, J. Phys. Chem. B **11**, 2173 (2011).

[57] D. Frenkel ,B. Smit, Understanding Molecular Simulation: From Algoritms to Applications (Academic Press, San Diego, 2002)

[58] N. Metropolis, A. W. Rosenbluth, M. N. Rosenbluth, A. H. Teller, E. Teller, J. Chem. Phys. **21**, 1087 (1953).

[59] E. G. Strekalova, M. G. Mazza, H. E. Stanley and G. Franzese, Phys. Rev. E **106**, 145701 (2011).

[60] E. G. Strekalova, M. G. Mazza, H. E. Stanley and G. Franzese, Phys. Rev. E **106**, 145701 (2011).

[61] E. G. Strekalova, D. Corradini, M. G. Mazza, S. V. Buldyrev, P. Gallo, G. Franzese, H. E. Stanley, J. Bio. Phys. **38**, 97 (2012).

[62] P. A. Netz, F. W. Starr, M. C. Barbosa and H. E. Stanley, Physica A **314**, 470 (2002).